inorganics

MDPI

Article

Electronic and Steric Effects on Oxygen Reactivities of NiFeSe Complexes Related to O_2-Damaged [NiFeSe]-Hydrogenases' Active Site

Yuchen Qiao [1,†], Enting Xu [2,†], Yameng Hao [2], Xuemei Yang [2,*] and Ming Ni [1,*]

[1] BGI Research, Shenzhen 518083, China; qiaoyuchen@genomics.cn
[2] School of Science, Harbin Institute of Technology (Shenzhen), Shenzhen 518055, China; 23S058068@stu.hit.edu.cn (E.X.); yameng.hao@alumni.epfl.ch (Y.H.)
* Correspondence: yangxuemei@hit.edu.cn (X.Y.); niming@mgi-tech.com (M.N.)
† These authors contributed equally to this work.

Abstract: Hydrogen has the potential to serve as a new energy resource, reducing greenhouse gas emissions that contribute to climate change. Natural hydrogenases exhibit impressive catalytic abilities for hydrogen production, but they often lack oxygen tolerance. Oxygen-tolerant hydrogenases can work under oxygen by reacting with oxygen to form inactive states, which can be reactivated to catalytic states by oxygen atom removal. Herein, we synthesized three NiFeSe complexes: ($NiSe(CH_3)FeCp$, $NiSe(CH_3)FeCp^*$ and $NiSe(Ph^{NMe2})FeCp$) with features of active sites of [NiFeSe]-H_2ases, which are the oxygen-tolerant hydrogenases, and we investigated the influence of electronic and steric factors on the oxygen reaction of these "biomimetic" complexes. In our research, we found that they react with oxygen, forming 1-oxygen species, which is related to the O_2-damaged [NiFeSe] active site. Through a comparative analysis of oxygen reactions, we have discovered that electronic factors and steric hindrance on Se play a significant role in determining the oxygen reactivity of NiFe complexes related to hydrogenases' active sites.

Keywords: hydrogenases biomimetics; oxygen tolerance; electronic effect; steric effect

Citation: Qiao, Y.; Xu, E.; Hao, Y.; Yang, X.; Ni, M. Electronic and Steric Effects on Oxygen Reactivities of NiFeSe Complexes Related to O_2-Damaged [NiFeSe]-Hydrogenases' Active Site. *Inorganics* **2024**, *12*, 163. https://doi.org/10.3390/inorganics12060163

Academic Editors: Sunčica Roca and Monika Kovačević

Received: 7 May 2024
Revised: 4 June 2024
Accepted: 7 June 2024
Published: 10 June 2024

1. Introduction

With the world's increasing reliance on fossil fuels, the rise of greenhouse gases and looming threat of climate change, there has been a drive to develop alternative fuels and environmentally friendly energy solutions. While solar, wind and water powers are clean, pollution-free and inexhaustible, unfortunately, they are unstable, variable and intermittent, which makes them less convenient, stable or efficient for widespread use. One of the solutions to address this problem is to store or convert these unstable natural energies into stable chemical bonds [1]. Among various energy carriers, hydrogen stands out due to its high energy per unit mass, cleanliness and zero carbon emission [2]. By utilizing hydrogen as an energy carrier, we can store the solar power and/or wind power into the dihydrogen bonds and release the energies when needed, such as in hydrogen vehicles.

So far, the best catalyst reported for hydrogen production has been platinum, which is both expensive and relatively scarce in terms of resources [3]. In the quest to design economic, efficient and sustainable catalysts for hydrogen production, natural catalysts, hydrogenases, have captured the interest of researchers. Hydrogenases, which are metalloenzymes, reversibly catalyze hydrogen gas from protons and electrons [4]. There are three main classes of hydrogenases, which include the [Fe]-, [FeFe]- and [NiFe] hydrogenases [5–10]. The active sites of these metalloenzymes are composed of inexpensive transition metals (iron and nickel), sulfur and simple diatomic ligands (CO and CN) that are effective for π-delocalization and H-bonding. While these natural catalysts demonstrate impressive catalytic abilities, a great challenge in utilizing hydrogenases or their models for industrial purposes is their low oxygen tolerance [11–13].

Oxygen tolerance has been used to describe the ability of hydrogenase to catalyze hydrogen oxidation or evolution under aerobic conditions, and more recently, it has been suggested to be limited for the catalysis of hydrogen oxidation only due to the catalysis possibility of oxygen-sensitive hydrogenases for hydrogen evolution [14]. However, a previous broader definition is still accepted and used in publications [15–17]. Some hydrogenases are reported to be oxygen-tolerant [18–20], and one possible mechanism is that oxygen-tolerant hydrogenases can react with oxygen to form an inactive state that can be subsequently recovered to rejoin the catalytic cycle [21,22]. Among the three classes of hydrogenases, it is reported that the [NiFe] hydrogenases have the highest oxygen tolerance [23]. Within the class of [NiFe] hydrogenases, there are two subclasses: [NiFeS] and the [NiFeSe] hydrogenases (Figure 1a, adapted from a previous study [24]). While sharing similar structures, one of the terminal cysteines in [NiFeS] hydrogenases is replaced by the selenocysteine in [NiFeSe] hydrogenases. However, this small modification results in the difference that the [NiFeSe] hydrogenases exhibit better recovery from oxygenation, suggesting a possible oxygen tolerance [15,16,25,26].

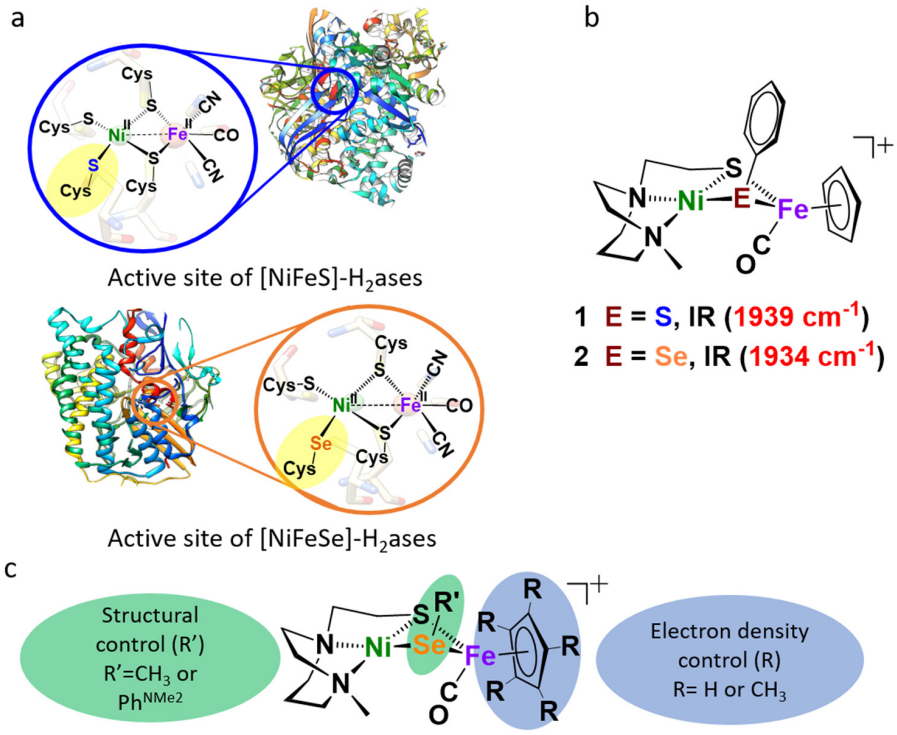

Figure 1. (**a**) The structures and active sites of [NiFeS] and [NiFeSe] hydrogenases. (**b**) A formatted structure of NiFe complexes related to [NiFe] hydrogenases' active sites (previous study [24]). (**c**) A sketch of modifications to the NiFeSe complex.

Although hydrogenases serve as natural catalysts for hydrogen production, they are inconvenient for direct industrial use due to the need for extraction and purification. Therefore, based on the active sites of hydrogenases, chemists and biochemists have designed and synthesized biomimetics [4,9,17,27,28] and bioinspired complexes [29–31], which show promise as catalysts. In addition, several biomimetics have been developed for the study of oxygenated [NiFeS] and [NiFeSe] hydrogenases, which helps to understand oxygen tolerance [24,32–36]. Specifically, in our previous study, the NiFe complex with selenium (Figure 1b) exhibited lower oxygen reactivity and higher oxygen recovery than its all-sulfur analog [24,35,36]. In the presence of oxygen, our sulfur complex was found to preferentially uptake two oxygen atoms that could not be recovered, while the selenium complex exhibited a preference for one oxygen atom that could be removed while adding a reducing agent.

To gain a deeper understanding of the O atom uptake, this study explores both steric hindrance on selenium and electronic modifications at the iron site. As depicted in Figure 1c, R′ was the phenyl group. However, R′ can also be substituted with other groups to change the chemical environment of the center atom, selenium. For example, once the R′ group was substituted by methyl, due to its smaller size, a less steric hindrance effect on the selenium atom should make it much easier to be attacked by oxygen. This would make the NiFeSe complex more oxygen-sensitive in order to generate more oxidated species once exposed under oxygen-containing environments (surprisingly, the results did not match with our expectations, *vide infra*). Additionally, the Cp ring that coordinated on the Fe side could be replaced by η^5-C_5Me_5 (Cp* ring). Because the Cp* group is the more electron-donating group compared to the Cp group, the electron density on Fe would increase and should be able to transfer to the chalcogenide, resulting in a higher electron density on the selenium side. Such an increase of the electron density on Se was expected to facilitate its 1-oxygen uptake, which was also confirmed by computational calculations. However, it should be pointed out that the great CO ligand was maintained, because it is not only a part for mimicking the hydrogenases' active site but also a great monitor for any structure change during the reaction, since it has an obvious band in the IR spectrum.

In summary, we anticipate that these modifications will alter the oxygen reactivity of the NiSeFe complex and lead to the formation of more 1-oxygen–selenium products. By comparing the oxygen reactions of these complexes, our goal is to analyze the effects of the electronic and steric factors on the O_2 reactivities of the NiFe complexes.

2. Results

2.1. Synthesis and Characterizations

Nickel dithiolate complexes are well-known for their reactivity as metalloligands, forming M-(μ_2-SR)$_2$-M′ bridges [37–39]. In 2010, Darensbourg's group reported several cleavage reactions of nickel bimetallic dimer $[NiN_2S]_2^{2+}$ using ligands such as imidazole, pyridine, etc. [40]. In our previous studies, those dimers were also able to be sliced by phenyl-based reductants, such as thiophenolate (SPh), benzeneselenolate (SePh) and their derivatives [24,35]. Based on these studies, the heterobimetallic complex was synthesized in our study. The $[NiNS_2]_2^{2+}$ dimer was divided by SeMe or $SePh^{NMe2}$, and the latter group was much bigger than the former, which could introduce a comparison of the steric hindrance in this system. The attained NiN_2S•SeMe was further reacted with $FeCp(CO)(CH_3CN)^+$ or $FeCp^*(CO)(CH_3CN)^+$ to obtain $NiSe(CH_3)FeCp$ or $NiSe(CH_3)FeCp^*$, respectively. This set, $NiSe(CH_3)FeCp/NiSe(CH_3)FeCp^*$, was chosen to investigate the electronic effect, since the Cp* was much more electron rich than Cp. The isolated NiN_2S•$SePh^{NMe2}$ was reacted with $FeCp(CO)(CH_3CN)^+$ to obtain $NiSe(Ph^{NMe2})FeCp$. This complex, in combination with $NiSe(CH_3)FeCp$, was used to analyze the steric effect on the O_2 reaction.

The synthesis routes and IR spectra of these heterobimetallics are shown in Figure 2. We hypothesized that, as the electron-donating ability of the substitution group on chalcogenide increases, more electron density should be able to transfer to iron through chemical bonds, which would result in more π-back-bonding formation between the iron atom and the coordinated carbon monoxide molecule and weaker carbon–oxygen triple bonds. This can be reflected by the decrease of the wavelength of carbon–oxygen bonding (v(CO)). In order to prove our hypothesis, we used an IR spectrophotometer to detect the v(CO) of each synthetic complex. The v(CO) of $NiSe(CH_3)FeCp^*$ was found at 1905 cm^{-1}, while $NiSe(CH_3)FeCp$ exhibited a value of v(CO) = 1929 cm^{-1}, which is in agreement with the fact that Cp* contributed more electrons due to its stronger electron-donating effect of methyl groups to the Fe atom rather than Cp. However, the electron-donating abilities of $SeCH_3$ (the top branch species in Figure 2) and $SePh^{NMe2}$ (the methyl group was substituted by a para-dimethyl amine benzyl group, the bottom branch species in Figure 2) were determined to be equivalent according to their identical v(CO) bands at 1929 cm^{-1}. Thus, when we compared these two complexes, we could exclude the electronic effect and consider the steric effect as the main factor.

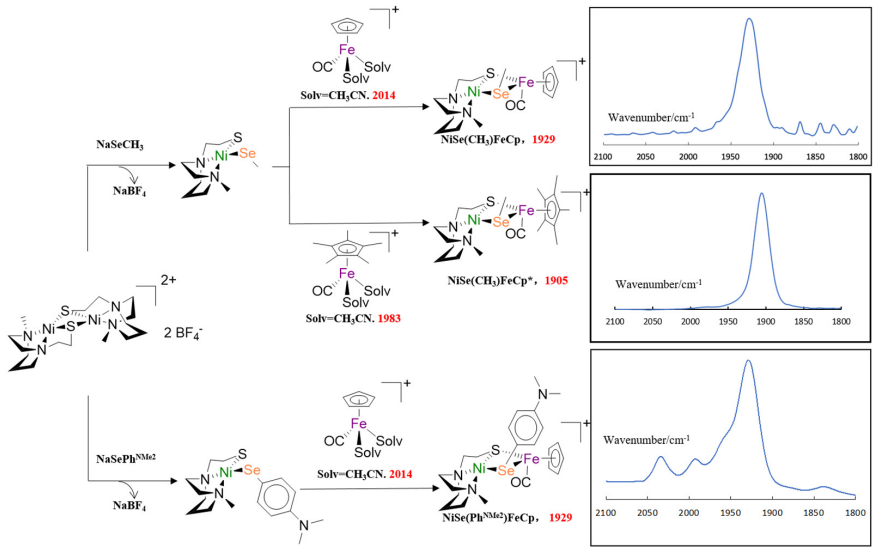

Figure 2. Synthetic routes of NiSeFe derivatives, their corresponding v(CO) values and IR spectra (the red numbers indicated the wavelength of the carbon–oxygen bond, v(CO)).

2.2. Oxygen Tolerance Test

At 22 °C, the heterobimetallic complexes were added to the O_2-saturated DCM solutions, and the reaction progresses were monitored by v(CO) using FTIR spectroscopy. We observed that the initially clear solution of complexes gradually transformed into a slightly cloudy solution. Following filtration, solvent removal and redissolving in DCM, the resulting solution was analyzed by high-resolution mass spectrometry. Based on previous studies, nickel–sulfur complexes were found to preferentially uptake two oxygen atoms, while nickel–selenium species exhibited a preference for one, suggesting the formation of a 1-oxygen uptake species in the three NiSeFe complexes [24,35]. Our previous work also showed that a 2-oxygen uptake NiSeFe complex, if generated, underwent comproportionating with the precursor to form two equivalents of the 1-oxygen complex. In this study, the NiSeFe complexes also followed the 1-oxygen uptake rule and matched with our expectations. It should be pointed out that, in our study, the O atom was bonded to Ni; however, in other, previous NiFe hydrogenase biomimetics studies, the O atom was also found to bind to the Fe moiety. For example, Ogo's group have published several significant studies on the O_2 reaction with biomimetic NiFe complexes in which the O_2 was activated to bond to Fe and perform O_2 reduction [41,42]. In our study, the O atom adopted a different insertion mode, although it was less reactive in O_2 reduction but it more gentle and potentially easier to be reversed to the original structure. Besides, while there was an oxidation state change in most reported studies, in our case, both the Fe and Ni maintained the two oxidation states.

Furthermore, it also suggested that the oxygen reactivity would be influenced by the electron-rich nature and steric hindrance of selenium, leading to the shorter reaction time and higher yield of oxygenates. The results of each O_2 reaction were characterized and analyzed *vide infra*.

2.2.1. The O_2 Reaction of NiSe(CH_3)FeCp

In the O_2 uptake reaction between O_2 and NiSe(R′)FeCp (R′ = Me or H), the time-dependent IR spectra for its product, the 1-oxygen uptake species, is presented in Figure 3. The reaction took approximately 35 min to reach completion. IR spectroscopy revealed the disappearance of the CO band at 1929 cm^{-1}, which represented the starting material, while a new band at 1947 cm^{-1} emerged along with the progression of the reaction. Upon the reaction lasting over 35 min, no further peak shifting and peak height changes could be observed. After isolation, the yield of oxygenated products, calculated by weight, was

approximately 30%. Furthermore, in the mass spectra, the parent peak and isotope bundle for this complex, which was 490.95 *m/z*, matched with the predicted value (Figure S1).

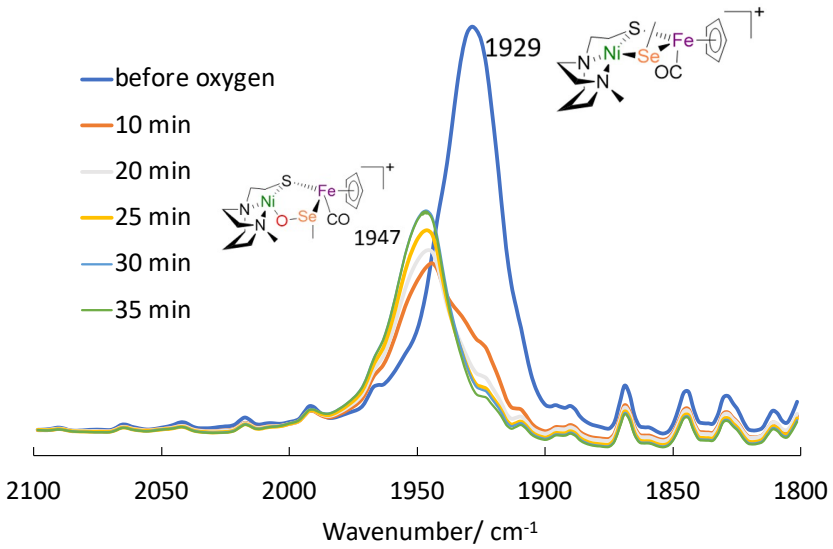

Figure 3. The IR spectra of the initial complex and final product of the O_2 uptake reaction between O_2 and NiSe(CH_3)FeCp.

2.2.2. The O_2 Reaction of NiSe(CH_3)FeCp*

Compared to the v(CO) band of NiSe(CH_3)FeCp mentioned above, the NiSe(CH_3)FeCp*, where the Cp group was switched to Cp* (C_5Me_5), exhibited the same optimized reaction time (35 min), whereas, based on the IR analysis as shown in Figure 4, the v(CO) band shifted from 1905 cm^{-1} to 1934 cm^{-1} after the reaction. It should be pointed out that this reaction was not finished until around 35 min, as shown in the inset of Figure 4b. The shoulder of 1905 (the band of the reactant) was still there at the reaction time of 25 min. Also, one thing to be pointed out in departure from all the other cases, is that the band of 1934 cm^{-1} was broader than those observed in the other oxygenated compounds, indicating that there might be more than one product; more details are analyzed below. The yield of the overall oxygenated products was approximately 58%.

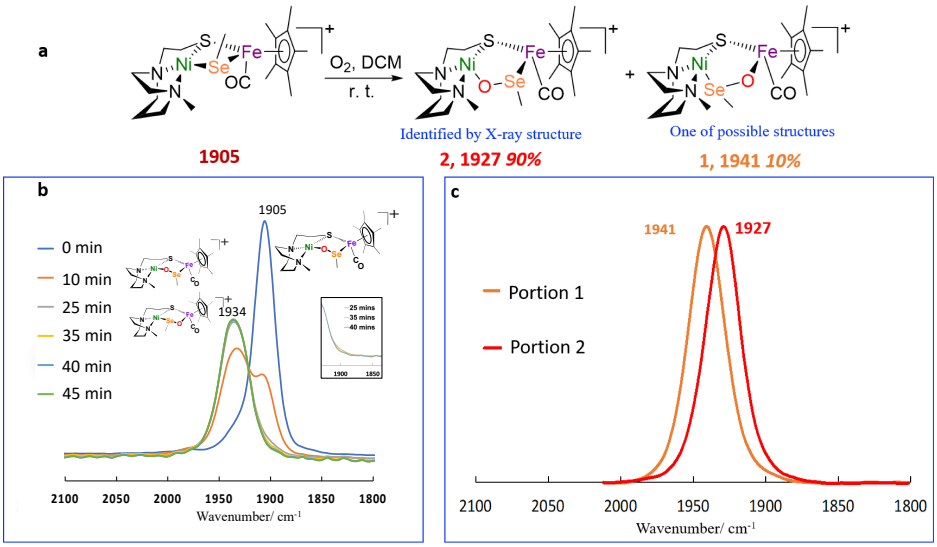

Figure 4. (**a**) Synthetic route of the O_2 uptake reaction between O_2 and NiSe(CH_3)FeCp*. (**b**) IR spectra of the initial complex and final product within the CO band range, the inset indicating the differences between 25, 35 and 40 min traces. (**c**) IR spectra of the two separated portions in the reaction mixture.

To separate the two components in the reaction mixture, we employed the column purification method by using a column filled by aluminum oxide (Al_2O_3). After the O_2 uptake reactions, dark-colored product mixture solutions were filtered and concentrated by vacuum vaporization. Subsequently, the volume-reduced filtrates were separately loaded onto different Al_2O_3 columns for further clean up.

We initially used pure DCM as the eluent to wash down portion 1 (v(CO) = 1941 cm^{-1}), which exhibited an orangish color. Then, a mixture of 10% methanol and 90% dichloromethane was used to elute down the following reddish-colored portion 2 (v(CO) = 1927 cm^{-1}). The yield ratio of portion 1 to portion 2 was approximately one to nine. It is important to note that, in order to visualize the difference better, the intensity of the v(CO) band at 1941 cm^{-1} was multiplied by nine in Figure 4c. We also attempted to influence the yield ratio using other O atom sources besides O_2, including hydrogen peroxide, trimethylamine N-oxide, tert-butyl OOH, etc., but those trials were all unsuccessful.

The parent peak and isotope bundles for this complex mixture, as shown in Figure S2a, matched with the predicted value 561.03 *m/z*. Isolated portion samples were also sent for analysis by mass spectrometry. As shown in Figure S2b,c, the same parent peak at 561.03 *m/z* was found in the $^+$ESI-MS spectra. The results strongly suggested that the two portions were likely isomers.

As shown in Figure 5a, the portion 2 species, NiOSeFe, still maintained the hetero-bimetallic structure, and the O atom was inserted into the Ni-Se bond, with the formation of new bond of Ni-O and O-Se due to the fact that the Ni-Se bond was broken. The distance between Ni and Fe was 3.604 Å, indicating that there was no metal–metal bond. From the side view of the structure, as shown in Figure 5b, it can be seen that the five-membered ring of Ni-O-Se-Fe-S was not in a plane but as a "crown". Such a structure might be due to the repelling of electrons or the steric hindrance. According to the structure of portion 2, we assume that the O atom was inserted between Fe and Se in portion 1 due to the higher nucleophile and oxygen reactivity of Se than S [26]. However, the structure of portion 1 was not confirmed, as it was not dominant in the mixture, and further studies are needed to confirm the structure.

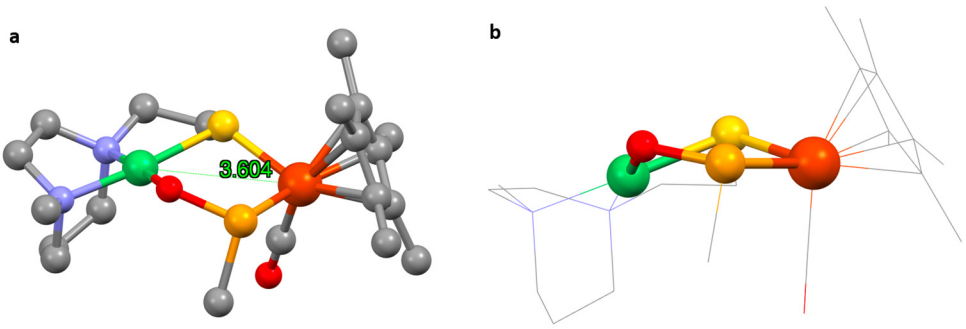

Figure 5. The crystal structure of portion 2, NiOSeFe, in a top-right view (**a**) and side view (**b**); hydrogens are omitted for clarity.

2.2.3. The O_2 Reaction of NiSe(Ph^{NMe2})FeCp

Same as the other biomimetics, the NiSe(Ph^{NMe2})FeCp was dissolved in the O_2-saturated DCM, and the oxygenation reaction was monitored by IR spectroscopy. According to the v(CO) in the IR spectra (Figure 6), within 40 min, the shift was transformed from 1929 cm^{-1} to 1950 cm^{-1}, with a final yield of 61% oxygenated product. Such product was further confirmed as the 1 oxygen uptake complex by mass spectrometry, as the *m/z* signals of 596.0067 matched perfectly with its calculated value (Figure S3).

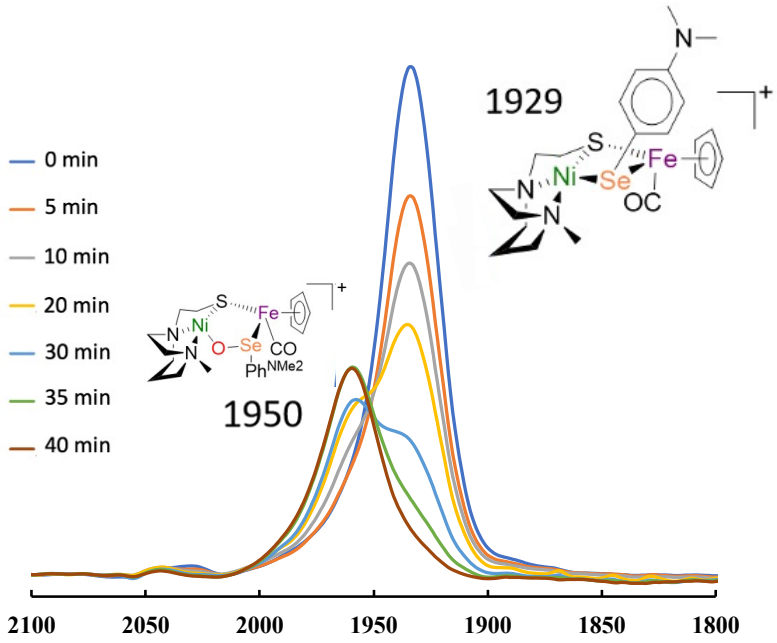

Figure 6. IR spectra of the O_2 reaction of NiSe(Ph^{NMe2})FeCp within the CO band range.

3. Discussion

Taking the three O_2 reactions mentioned above as the conclusion, their reaction parameters are summarized in Table 1. From the reaction time, there was no obvious difference between the three reactions. It should be pointed out that, different from the O_2 bubbling method that some literature has reported (our previous studies [24,35] (from M. Darensbourg's team) included), in this study, we used the O_2-saturated method, dissolving oxygen in DCM solution before the O_2 reaction. Such a modification excluded that the speed of O_2 diffusion in the solution affected the O_2 reaction. The O_2 reactions in this study all finished in 35–40 min, indicating that the differences in electronic or steric hindrance did not affect the reaction time in oxygenation.

Table 1. The overall oxygen reactions of the three NiSeFe complexes.

R′-R	Reaction Time (min)	ν_1(CO) (cm^{-1})	ν_2(CO) (cm^{-1})	Yield (%)
CH_3-Cp	35	1929	1947	30 ± 4
CH_3-Cp*	35	1905	1941, 1927	56 ± 3
Ph^{NMe2}-Cp	40	1929	1950	61 ± 4

3.1. Electronic Effect on the Fe Moiety

With the experimental data of NiSe(CH_3)FeCp and NiSe(CH_3)FeCp* in hand, we could analyze how different substitution groups on Fe caused their distinct O_2 uptake reactivity. Consistent with previous studies, mass spectrometry analysis proved that 1-O uptake was the only oxygenating type of the nickel–selenium complexes [24,35]. However, contrary to our expectations, the oxygen uptake reaction time period of electrons enriched in NiSe(CH_3)FeCp* did not vary at all. There are two assumptions that can be used to explain this experimental phenomenon. First, the electron density generated by the substituted selenium center was sufficient enough to provide the optimized conditions for oxygen to be added, regardless of the donor group on Fe. This step was not the time-limited step for this oxygenating reaction. Second, due to the relatively far distance between the Cp ring and reaction center, selenium, the change in electron density of the iron atom might not have influenced the oxygenating reaction rates at a significant level.

Although there was no substantial variance on the reaction rates of the Cp and Cp* complexes, the yields of their oxygenized compounds still diverged from each other (56%

vs. 30%). Based on our previous DFT (density functional theory) studies, the O_2 uptake intermediates were proposed to be Ni(III)-OO, with bond breaking of Ni-S or Ni-Se at the same time [35]. Despite no oxygen atom being directly added onto the Fe site, it played the role as a Se-R stabilizer and reaction accelerator, which promoted the oxygen reduction progress. For Cp* substitution, the existing five methyl groups on the five-member ring enlarged the electron density of Fe, which might better facilitate an O_2 reduction and steady its reaction intermediate.

To further compare the oxidation reactions of NiSe(CH_3)FeCp and NiSe(CH_3)FeCp*, DFT computations were also performed in this study to address the thermodynamic driving forces for O atom uptake and the different types of oxidized products. As summarized in Figure 7, the free energies, ΔG°, for O insertion into the Ni-Se and Fe-Se bonds in NiSe(CH_3)FeCp were −24.1 and −6.2 kcal/mol, while, in NiSe(CH_3)FeCp*, the numbers were −29.9 and −9.1 kcal/mol. These numbers indicated that the oxidation reaction of NiSe(CH_3)FeCp* was easier than NiSe(CH_3)FeCp, with more negative free energies (ca. −3 to 5 kcal/mol), which was what we expected, since Cp* causes the Fe moiety to obtain a higher electron density than Cp, and it matched with our experimental results that the oxidation product yield of NiSe(CH_3)FeCp* (56%) was higher than the products of NiSe(CH_3)FeCp (30%). Compared to the 2-O insertion type, in both cases, the O atom thermodynamically preferred to insert between Ni and Se rather than Fe and Se.

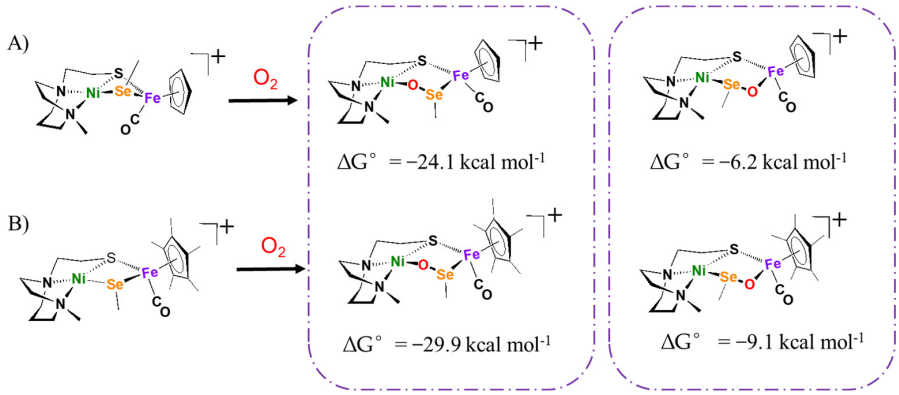

Figure 7. DFT calculated the free energy values, ΔG°, for comparison of the oxygen uptake reactions of (**A**) NiSe(CH_3)FeCp and (**B**) the NiSe(CH_3)FeCp*.

3.2. Intermediate Delocalization Effect on Se

Although the reaction time (35–40 min) remained similar, the yield of NiOSe(Ph^{NMe2})FeCp (61%) was much greater than NiOSe(CH_3)FeCp (30%). Considering the fact that both analogs showed equal C≡O IR vibration values, those two groups' electron-providing capabilities were comparable. Under this circumstance, to some degree, we could compare the steric hindrance between them. However, it should be pointed out that the $PhNMe_2$ group was not suitable to investigate the purely steric effects, and the synthesis of new complexes with more hindered alkyl chains should be explored to better investigate this aspect.

Surprisingly, the experiments aforementioned contradicted our initial thought that the higher yield should result from less steric hindrance, which would make the oxygen molecule proximate Se easier. Due to the possibility of an electronic effect as well, in order to explain why CH_3 and Ph^{NMe2} revealed similar reaction rates but distinct yields, we looked at if any structural features would facilitate the formation of NiOSe(Ph^{NMe2})FeCp. As mentioned in the previous paragraph, the intermediate of such an oxygen uptake reaction was likely to be a peroxide species, which is a kind of radical species. Compared to Se-Ph^{NMe2}, where the radical had a chance to delocalize on the benzene ring and the *para*-nitrogen atom, which led to the increasing of the intermediate stability, the methyl group, due to its relatively small size and the absence of an electron delocalization ability, could not offer any protection for the intermediate radical when reacted with other radical quenchers

in the reaction mixture. It is very likely that the radical was quickly consumed by the cations and anions that existed everywhere in the solvent to form variable byproducts, such as Se-Se and di-selenide, after the peroxide intermediates had formed. The demonstrated two-isomer formation additionally supported our assumption. In contrast, in the amino phenyl group case, the •Se- Ph^{NMe2} radical was able to delocalize in the π system in order to prolong its lifetime, which would definitely drive the reaction in the single-oxygen uptake direction. Further experiments will be necessary to prove the aforementioned assumptions.

4. Materials and Methods

4.1. General Materials and Techniques

All reagents and solvents were purchased from Sigma-Aldrich (St. Louis, MO, USA), VWR (Radnor, PA, USA) or Thermo Fisher Scientific (Waltham, MA, USA). All purified organic solvents were further dehydrated by a manual solvent purification system (M. Braun Inc., Stratham, NH, USA) packed with Alcoa F200-activated alumina desiccant. All reactions (except the O_2 oxidation reactions) and operations were performed in a glovebox or on a double-manifold Schlenk vacuum line under an inert gas supply.

4.2. IR Spectrometry Analysis and Reaction Progress Monitoring

Solution infrared spectra were evaluated on a Tensor 37 Fourier-transform IR (FTIR) spectrometer (Bruker, Billerica, MA, USA) using a CaF_2 cell with a 0.2 mm path length. Oxygenation completion was monitored by the change in the IR absorption peaks that corresponded to the C≡O stretching area. The time period the reaction lasted was recorded to represent the optimized reaction rate when there was no change in the intensity for both the reactant and product's C≡O stretching bands.

4.3. X-ray Structure Analysis and Data Processing

Data collections for X-ray structure determination were carried out using APEX2[4] or Venture (Bruker, Billerica, MA, USA) with a graphite mono-chromated radiation source (λ = 0.71073 Å). All crystals were coated in paraffin oil and mounted on a nylon loop and placed under streaming nitrogen gas (110/150K). The structures were solved by direct methods (SHELXS-97) and refined by standard Fourier techniques against F square with a full-matrix least squares algorithm using SHELXL-97 and the WinGX (1.80.05) software package. All non-hydrogen atoms were refined anisotropically. Hydrogen atoms were placed in calculated positions and refined with a riding model. Graphical representations were prepared with ORTEP-III. Crystallographic data (including structure factors) were deposited with the Cambridge Crystallographic Data Centre (no. 2035045).

4.4. DFT Calculation Methods

All of the spin-polarized calculations were based on density functional theory (DFT) and performed by the DMol3 package. The GGA (generalized gradient approximation) in the Perdew–Burke–Ernzerhof form, DSPP (semi-core pseudopotential method) with the double numerical basis sets and the polarization functional (DNP) were chosen for the calculations. The dispersion interaction was accounted by a DFT-D correction with a Grimme scheme. The SCF convergence for every electronic energy was set as 1.0×10^{-7} Ha. The geometry optimization convergence criteria were set up as follows: 1.0×10^{-7} Ha for the energy, 0.001 Ha $Å^{-1}$ for the force and 0.001 Å for displacement, respectively. The free energy (G) for the elemental reaction step was analyzed by the formula

$$G = E + EZPE - TS$$

where E is the total energy of the structures, EZPE is the zero-point energy, T is the temperature and S the change in entropy. Finally, the reaction energies (G) of different intermediates were defined by the formula

$$\Delta G = Gi - Greactant$$

where Gi is the energy of the intermediate, and Greactant is the total energy of the reactant.

5. Conclusions

In our work, we synthesized and analyzed three different NiSeFe heterobimetallics in order to further investigate the buried mystery of what factors make nickel–selenium hydrogenase exhibit a certain oxygen tolerance. The O_2 uptake of the three "biomimetics" are conducted to compare the electronic and steric effects, as well as structural comparisons. Although similar reaction times were observed for all complexes to achieve the optimal yields, the actual yields differed. A higher yield of 1-oxygen species was observed when the Se-Ph^{NMe2} and Cp* groups were present in the biomimetic organometallic complexes. Therefore, we drew the following conclusions:

(a) The three complexes can react with oxygen to form a 1-oxygen species, which is related to the O_2-damaged [NiFeSe] hydrogenases' active sites.
(b) Since NiSe(Ph^{NMe2})FeCp and NiSe(CH_3)FeCp shared identical ν(CO) values, Ph^{NMe2} had an electron-donating ability equivalent to that of the CH_3 group. Cp* demonstrated better electron-donating properties than Cp, resulting in increased π-back-bonding from Fe to CO and a higher oxygen reactivity.
(c) The -SeMe group, due to its greater lability and reduced steric bulk, produced a pair of isomers that were detected at different IR wavenumbers.
(d) The -SeMe variant, owing to its small size and limited electron delocalization ability of the methyl group, exhibited lower oxygen reactivity—in other words, more decomposed byproducts and a lower yield of 1-oxygen uptake species.
(e) Besides all the effects aforementioned, other factors might influence the complex oxidation reactivity.

In conclusion, first, we found all the complexes could be oxygenated to 1-oxygen species, which had the potential to be recovered. Then, through a comparative analysis of oxygen reactions, we discovered that the higher electron donation and steric hindrance on selenium could increase the oxygen reactivity of our hydrogenase biomimetics. We hope our study can become a modest spur to stimulate researchers to dig deeper into the hydrogenase oxygen tolerance area to discover more appreciated charities to promote the study and production of hydrogen energy.

Supplementary Materials: The following supporting information can be downloaded at https://www.mdpi.com/article/10.3390/inorganics12060163/s1: Figure S1: High-resolution $^+$ESI-MS of the 1-O uptake of NiSe(CH_3)FeCp. Figure S2: High-resolution $^+$ESI-MS of the 1-O uptake of NiSe(CH_3)FeCp*. Figure S3: High-resolution $^+$ESI-MS of the 1-O uptake of NiSe(Ph^{NMe2})FeCp.

Author Contributions: Conceptualization, X.Y. and M.N.; methodology, Y.Q., E.X. and X.Y.; software, E.X. and Y.H.; validation, Y.Q., E.X. and X.Y.; formal analysis, Y.Q. and Y.H.; investigation, Y.Q. and Y.H.; resources, Y.Q. and Y.H.; data curation, Y.Q. and E.X.; writing—original draft preparation, X.Y.; writing—review and editing, Y.Q., Y.H. and M.N.; visualization, Y.Q.; supervision, X.Y. and M.N.; project administration, X.Y. and M.N.; funding acquisition, Y.Q., X.Y. and M.N. All authors have read and agreed to the published version of the manuscript.

Funding: This research was funded by the Shenzhen Science and Technology Innovation Commission, grant number RCBS20221008093334080, the Development and Reform Commission of Shenzhen, grant number XMHT20220103004, and the Shenzhen Science and Technology Program, grant number JCYJ20230807153500001.

Data Availability Statement: The original contributions presented in the study are included in the article/Supplementary Materials; further inquiries can be directed to the corresponding author/s.

Conflicts of Interest: Yuchen Qiao and Ming Ni are employed by the company BGI Research. All the authors declare no conflicts of interest.

References

1. Su, L.; Ajo-Franklin, C.M. Reaching full potential: Bioelectrochemical systems for storing renewable energy in chemical bonds. *Curr. Opin. Biotechnol.* **2019**, *57*, 66–72. [CrossRef] [PubMed]
2. Sarmah, M.K.; Singh, T.P.; Kalita, P.; Dewan, A. Sustainable hydrogen generation and storage—A review. *RSC adv.* **2023**, *13*, 25253–25275. [CrossRef] [PubMed]
3. Gao, X.; Dai, S.; Teng, Y.; Wang, Q.; Zhang, Z.; Yang, Z.; Park, M.; Wang, H.; Jia, Z.; Wang, Y.; et al. Ultra-Efficient and Cost-Effective Platinum Nanomembrane Electrocatalyst for Sustainable Hydrogen Production. *NanoMicro Lett.* **2024**, *16*, 108. [CrossRef] [PubMed]
4. Lubitz, W.; Ogata, H.; Rüdiger, O.; Reijerse, E. Hydrogenases. *Chem. Rev.* **2014**, *114*, 4081–4148. [CrossRef]
5. Heinekey, D.M. Hydrogenase enzymes: Recent structural studies and active site models. *J. Organomet. Chem.* **2009**, *694*, 2671–2680. [CrossRef]
6. Ogata, H.; Hirota, S.; Nakahara, A.; Komori, H.; Shibata, N.; Kato, T.; Kano, K.; Higuchi, Y. Activation process of [NiFe] hydrogenase elucidated by high-resolution X-ray analyses: Conversion of the ready to the unready state. *Structure* **2005**, *13*, 1635–1642. [CrossRef]
7. Shima, S.; Thauer, R.K. A third type of hydrogenase catalyzing H2 activation. *Chem. Rec.* **2007**, *7*, 37–46. [CrossRef]
8. Volbeda, A.; Amara, P.; Darnault, C.; Mouesca, J.M.; Parkin, A.; Roessler, M.M.; Armstrong, F.A.; Fontecilla-Camps, J.C. X-ray crystallographic and computational studies of the O2-tolerant [NiFe]-hydrogenase 1 from Escherichia coli. *Proc. Natl. Acad. Sci. USA* **2012**, *109*, 5305–5310. [CrossRef]
9. Wombwell, C.; Reisner, E. Synthetic Active Site Model of the [NiFeSe] Hydrogenase. *Chemistry* **2015**, *21*, 8096–8104. [CrossRef]
10. Wombwell, C.; Reisner, E. Synthesis, structure and reactivity of Ni site models of [NiFeSe] hydrogenases. *Dalton Trans.* **2014**, *43*, 4483–4493. [CrossRef]
11. Buhrke, T.; Lenz, O.; Krauss, N.; Friedrich, B. Oxygen tolerance of the H2-sensing [NiFe] hydrogenase from Ralstonia eutropha H16 is based on limited access of oxygen to the active site. *J. Biol. Chem.* **2005**, *280*, 23791–23796. [CrossRef] [PubMed]
12. Dey, S.; Rana, A.; Crouthers, D.; Mondal, B.; Das, P.K.; Darensbourg, M.Y.; Dey, A. Electrocatalytic O2 Reduction by [Fe-Fe]-Hydrogenase Active Site Models. *J. Am. Chem. Soc.* **2014**, *136*, 8847–8850. [CrossRef] [PubMed]
13. Frielingsdorf, S.; Fritsch, J.; Schmidt, A.; Hammer, M.; Löwenstein, J.; Siebert, E.; Pelmenschikov, V.; Jaenicke, T.; Kalms, J.; Rippers, Y.; et al. Reversible [4Fe-3S] cluster morphing in an O(2)-tolerant [NiFe] hydrogenase. *Nat. Chem. Biol.* **2014**, *10*, 378–385. [CrossRef] [PubMed]
14. Shafaat, H.S.; Rüdiger, O.; Ogata, H.; Lubitz, W. [NiFe] hydrogenases: A common active site for hydrogen metabolism under diverse conditions. *Biochim. Biophys. Acta* **2013**, *1827*, 986–1002. [CrossRef] [PubMed]
15. Marques, M.C.; Tapia, C.; Gutiérrez-Sanz, O.; Ramos, A.R.; Keller, K.L.; Wall, J.D.; De Lacey, A.L.; Matias, P.M.; Pereira, I.A.C. The direct role of selenocysteine in [NiFeSe] hydrogenase maturation and catalysis. *Nat. Chem. Biol.* **2017**, *13*, 544–550. [CrossRef] [PubMed]
16. Barbosa, T.M.; Baltazar, C.S.A.; Cruz, D.R.; Lousa, D.; Soares, C.M. Studying O(2) pathways in [NiFe]- and [NiFeSe]-hydrogenases. *Sci. Rep.* **2020**, *10*, 10540. [CrossRef]
17. Ahmed, M.E.; Dey, S.; Darensbourg, M.Y.; Dey, A. Oxygen-Tolerant H2 Production by [FeFe]-H2ase Active Site Mimics Aided by Second Sphere Proton Shuttle. *J. Am. Chem. Soc.* **2018**, *140*, 12457–12468. [CrossRef]
18. Pandelia, M.E.; Fourmond, V.; Tron-Infossi, P.; Lojou, E.; Bertrand, P.; Léger, C.; Giudici-Orticoni, M.T.; Lubitz, W. Membrane-bound hydrogenase I from the hyperthermophilic bacterium Aquifex aeolicus: Enzyme activation, redox intermediates and oxygen tolerance. *J. Am. Chem. Soc.* **2010**, *132*, 6991–7004. [CrossRef]
19. Parkin, A.; Goldet, G.; Cavazza, C.; Fontecilla-Camps, J.C.; Armstrong, F.A. The difference a Se makes? Oxygen-tolerant hydrogen production by the [NiFeSe]-hydrogenase from Desulfomicrobium baculatum. *J. Am. Chem. Soc.* **2008**, *130*, 13410–13416. [CrossRef]
20. Lenz, O.; Lauterbach, L.; Frielingsdorf, S. O_2-tolerant [NiFe]-hydrogenases of Ralstonia eutropha H16: Physiology, molecular biology, purification, and biochemical analysis. *Methods Enzymol.* **2018**, *613*, 117–151. [CrossRef]
21. Barilone, J.L.; Ogata, H.; Lubitz, W.; van Gastel, M. Structural differences between the active sites of the Ni-A and Ni-B states of the [NiFe] hydrogenase: An approach by quantum chemistry and single crystal ENDOR spectroscopy. *Phys. Chem. Chem. Phys.* **2015**, *17*, 16204–16212. [CrossRef] [PubMed]
22. Wulff, P.; Day, C.C.; Sargent, F.; Armstrong, F.A. How oxygen reacts with oxygen-tolerant respiratory [NiFe]-hydrogenases. *Proc. Natl. Acad. Sci. USA* **2014**, *111*, 6606–6611. [CrossRef] [PubMed]
23. Baltazar, C.S.A.; Marques, M.C.; Soares, C.M.; DeLacey, A.M.; Pereira, I.A.C.; Matias, P.M. Nickel–Iron–Selenium Hydrogenases—An Overview. *Eur. J. Inorg. Chem.* **2011**, *2011*, 948–962. [CrossRef]
24. Yang, X.; Elrod, L.C.; Reibenspies, J.H.; Hall, M.B.; Darensbourg, M.Y. Oxygen uptake in complexes related to [NiFeS]- and [NiFeSe]-hydrogenase active sites. *Chem. Sci.* **2019**, *10*, 1368–1373. [CrossRef] [PubMed]
25. Wombwell, C.; Caputo, C.A.; Reisner, E. [NiFeSe]-hydrogenase chemistry. *Acc. Chem. Res.* **2015**, *48*, 2858–2865. [CrossRef] [PubMed]
26. Reich, H.J.; Hondal, R.J. Why Nature Chose Selenium. *ACS Chem. Biol.* **2016**, *11*, 821–841. [CrossRef] [PubMed]
27. Rauchfuss, T.B. Diiron azadithiolates as models for the [FeFe]-hydrogenase active site and paradigm for the role of the second coordination sphere. *Acc. Chem. Res.* **2015**, *48*, 2107–2116. [CrossRef] [PubMed]

28. Liu, T.; Li, B.; Singleton, M.L.; Hall, M.B.; Darensbourg, M.Y. Sulfur oxygenates of biomimetics of the diiron subsite of the [FeFe]-hydrogenase active site: Properties and oxygen damage repair possibilities. *J. Am. Chem. Soc.* **2009**, *131*, 8296–8307. [CrossRef]
29. Ahmed, M.E.; Nayek, A.; Križan, A.; Coutard, N.; Morozan, A.; Ghosh Dey, S.; Lomoth, R.; Hammarström, L.; Artero, V.; Dey, A. A Bidirectional Bioinspired [FeFe]-Hydrogenase Model. *J. Am. Chem. Soc.* **2022**, *144*, 3614–3625. [CrossRef]
30. Leone, L.; Sgueglia, G.; La Gatta, S.; Chino, M.; Nastri, F.; Lombardi, A. Enzymatic and Bioinspired Systems for Hydrogen Production. *Int. J. Mol. Sci.* **2023**, *24*, 8605. [CrossRef]
31. Caputo, C.A.; Gross, M.A.; Lau, V.W.; Cavazza, C.; Lotsch, B.V.; Reisner, E. Photocatalytic hydrogen production using polymeric carbon nitride with a hydrogenase and a bioinspired synthetic Ni catalyst. *Angew. Chem. Int. Ed. Engl.* **2014**, *53*, 11538–11542. [CrossRef] [PubMed]
32. Ogo, S. H2 and O2 activation by [NiFe]hydrogenases—Insights from model complexes. *Coord. Chem. Rev.* **2017**, *334*, 43–53. [CrossRef]
33. Lindenmaier, N.J.; Wahlefeld, S.; Bill, E.; Szilvási, T.; Eberle, C.; Yao, S.; Hildebrandt, P.; Horch, M.; Zebger, I.; Driess, M. An S-Oxygenated [NiFe] Complex Modelling Sulfenate Intermediates of an O2-Tolerant Hydrogenase. *Angew. Chem. Int. Ed.* **2017**, *56*, 2208–2211. [CrossRef] [PubMed]
34. Song, L.-C.; Chen, W.; Feng, L. Two heterodinuclear NiFe-based sulfenate complexes mimicking an S-oxygenated intermediate of an O2-tolerant [NiFe]-H2ase: Synthesis, structures, and reactivity. *New J. Chem.* **2020**, *44*, 14015–14023. [CrossRef]
35. Yang, X.; Elrod, L.C.; Le, T.; Vega, V.S.; Naumann, H.; Rezenom, Y.; Reibenspies, J.H.; Hall, M.B.; Darensbourg, M.Y. Controlling O(2) Reactivity in Synthetic Analogues of [NiFeS]- and [NiFeSe]-Hydrogenase Active Sites. *J. Am. Chem. Soc.* **2019**, *141*, 15338–15347. [CrossRef] [PubMed]
36. Yang, X.; Darensbourg, M.Y. The roles of chalcogenides in O(2) protection of H(2)ase active sites. *Chem. Sci.* **2020**, *11*, 9366–9377. [CrossRef]
37. Denny, J.A.; Darensbourg, M.Y. Metallodithiolates as ligands in coordination, bioinorganic, and organometallic chemistry. *Chem. Rev.* **2015**, *115*, 5248–5273. [CrossRef]
38. Fogeron, T.; Todorova, T.K.; Porcher, J.-P.; Gomez-Mingot, M.; Chamoreau, L.-M.; Mellot-Draznieks, C.; Li, Y.; Fontecave, M. A Bioinspired Nickel(bis-dithiolene) Complex as a Homogeneous Catalyst for Carbon Dioxide Electroreduction. *ACS Catal.* **2018**, *8*, 2030–2038. [CrossRef]
39. Ghosh, P.; Quiroz, M.; Wang, N.; Bhuvanesh, N.; Darensbourg, M.Y. Complexes of MN2S2·Fe(η5-C5R5)(CO) as platform for exploring cooperative heterobimetallic effects in HER electrocatalysis. *Dalton Trans.* **2017**, *46*, 5617–5624. [CrossRef]
40. Jenkins, R.M.; Singleton, M.L.; Leamer, L.A.; Reibenspies, J.H.; Darensbourg, M.Y. Orientation and stereodynamic paths of planar monodentate ligands in square planar nickel N2S complexes. *Inorg. Chem.* **2010**, *49*, 5503–5514. [CrossRef]
41. Kishima, T.; Matsumoto, T.; Nakai, H.; Hayami, S.; Ohta, T.; Ogo, S. A High-Valent Iron(IV) Peroxo Core Derived from O2. *Angew. Chem. Int. Ed.* **2016**, *55*, 724–727. [CrossRef] [PubMed]
42. Isegawa, M.; Sharma, A.K.; Ogo, S.; Morokuma, K. DFT Study on Fe(IV)-Peroxo Formation and H Atom Transfer Triggered O2 Activation by NiFe Complex. *Organometallics* **2018**, *37*, 1534–1545. [CrossRef]